Biochimica et Biophysica Acta 1837 (2014) 33–43

Contents lists available at ScienceDirect

Biochimica et Biophysica Acta

journal homepage: www.elsevier.com/locate/bbabio

The C-terminal extension of bacterial flavodoxin-reductases: Involvement in the hydride transfer mechanism from the coenzyme

Ana Bortolotti [a,1], Ana Sánchez-Azqueta [b,1], Celia M. Maya [c], Adrián Velázquez-Campoy [b,d], Juan A. Hermoso [e], Milagros Medina [b,*], Néstor Cortez [a,**]

[a] Instituto de Biología Molecular y Celular de Rosario, Universidad Nacional de Rosario & CONICET, Rosario, Argentina
[b] Departamento de Bioquímica y Biología Molecular, Facultad de Ciencias e Instituto de Biocomputación y Física de Sistemas Complejos (BIFI)-Unidad Asociada IQFR, Universidad de Zaragoza, Zaragoza, Spain
[c] Instituto de Investigaciones Químicas (IIQ), Universidad de Sevilla-CSIC, Sevilla, Spain
[d] Fundacion ARAID, Gobierno de Aragón, Spain
[e] Departamento de Cristalografía y Biología Estructural, Instituto de Química Física Rocasolano (IQFR), CSIC, Madrid, Spain

ARTICLE INFO

Article history:
Received 11 June 2013
Received in revised form 26 August 2013
Accepted 28 August 2013
Available online 6 September 2013

Keywords:
Ferredoxin (flavodoxin)-NADP$^+$ reductase
Catalytic efficiency
Crystal structure
Hydride transfer

ABSTRACT

To study the role of the mobile C-terminal extension present in bacterial class of plant type NADP(H):ferredoxin reductases during catalysis, we generated a series of mutants of the *Rhodobacter capsulatus* enzyme (*Rc*FPR). Deletion of the six C-terminal amino acids beyond alanine 266 was combined with the replacement A266Y, emulating the structure present in plastidic versions of this flavoenzyme. Analysis of absorbance and fluorescence spectra suggests that deletion does not modify the general geometry of FAD itself, but increases exposure of the flavin to the solvent, prevents a productive geometry of FAD:NADP(H) complex and decreases the protein thermal stability. Although the replacement A266Y partially coats the isoalloxazine from solvent and slightly restores protein stability, this single change does not allow formation of active charge-transfer complexes commonly present in the wild-type FPR, probably due to restraints of C-terminus pliability. A proton exchange process is deduced from ITC measurements during coenzyme binding. All studied *Rc*FPR variants display higher affinity for NADP$^+$ than wild-type, evidencing the contribution of the C-terminus in tempering a non-productive strong (rigid) interaction with the coenzyme. The decreased catalytic rate parameters confirm that the hydride transfer from NADPH to the flavin ring is considerably hampered in the mutants. Although the involvement of the C-terminal extension from bacterial FPRs in stabilizing overall folding and bent-FAD geometry has been stated, the most relevant contributions to catalysis are modulation of coenzyme entrance and affinity, promotion of the optimal geometry of an active complex and supply of a proton acceptor acting during coenzyme binding.

1. Introduction

Plant-type ferredoxin/flavodoxin:NADP(H) reductases (FNRs) are monomeric FAD-dependent enzymes that catalyse the electron transfer from reduced ferredoxin (Fd), or flavodoxin (Fld), to NADP$^+$ in the photosynthetic electron transport chain, or the reverse reduction providing low-potential electrons for a variety of reactions such as nitrogen fixation, sulphur assimilation and amino acid biosynthesis [1–7]. Sequence and structural analysis of different FNRs led to subdivision of the family into two classes: the plastidic type, consistent of proteins present in cyanobacteria and chloroplasts from plants and algae, and the bacterial type enclosing flavodoxin-NADPH reductases, known as FPRs, present in eubacteria [2,8,9]. In organisms displaying oxygenic photosynthesis, the reactions catalysed by FNR are displaced towards NADP$^+$ reduction, with turnovers in the 200–600 s^{-1} range for the plastidic enzymes [10–12]. Differently, bacterial FPRs catalyse the reduction of the protein substrate by NADPH with estimated rates in the 1–200 s^{-1} range

Abbreviations: FAD and FADH$^-$, oxidised and two-electron reduced forms of the flavin adenine dinucleotide; WT, wild-type; CTC, charge transfer complex; HT, hydride transfer; ITC, isothermal titration calorimetry; FNR/FPR, plastidic/bacterial ferredoxin-NADP$^+$ reductase; FPR_{ox}, FPR in the oxidised state; r.m.s.d., root mean square deviation; NMN, nicotinamide mononucleotide portion of NADP$^+$/H; 2′P-AMP, 2′-phospho-AMP portion of NADP$^+$/H; $k_{A \to B}$, $k_{B \to C}$, apparent conversion rate constants derived by global analysis; k_{HT}, HT first-order rate constant; K_d, dissociation constant of the FPR_{ox}:NADP$^+$ complex; K_d^{NADPH}, dissociation constant of the FNR_{ox}:NADPH complex

* Correspondence to: M. Medina, Departamento de Bioquímica y Biología Molecular y Celular, Facultad de Ciencias. Universidad de Zaragoza, 50009-Zaragoza, Spain. Tel.: +34 976762476; fax: +34 976762123.
** Correspondence to: N. Cortez, IBR Instituto de Biología Molecular y Celular de Rosario (CONICET y Universidad Nacional de Rosario), Fac. Cs. Bioquímicas y Farmacéuticas, Suipacha 531, S2002LRK Rosario, Argentina. Tel.: +54 3414350596; fax: +54 3414390465.
E-mail addresses: mmedina@unizar.es (M. Medina), cortez@ibr-conicet.gov.ar (N. Cortez).

[1] These authors contributed equally to the manuscript and must be both considered as first author.

0005-2728/$ – see front matter © 2013 Elsevier B.V. All rights reserved.
http://dx.doi.org/10.1016/j.bbabio.2013.08.008

[6,7,13–17] being this activity in eubacteria related to different metabolic pathways including nitrogen fixation and response to oxidative stress [4,6,14].

The catalytic mechanism for plastidic FNRs has been thoroughly characterised using enzymes from spinach, pea and the cyanobacterium *Anabaena*. A sequential ordered mechanism of catalysis was early proposed, including the ternary complex as required intermediate, and being binding of $NADP^+$ the leader substrate by increasing the rate of FNR reduction from Fd_{rd} and facilitating dissociation of Fd_{ox} [18]. Later on, residues involved in the stabilisation of the ternary catalytic complex and particularly in the allocation of the nucleotide on the enzyme structure to produce the catalytically competent conformation have been identified [3,19–23]. The FNR/FPR ability to split electrons between obligatory two-electrons and mono-electron carriers is a consequence of the biochemical properties within the protein environment of their FAD prosthetic group. Thus, its oxido-reduction properties and the optimal disposition of the isoalloxazine and the nicotinamide reacting rings during the hydride transfer (HT) event are highly modulated by the interactions established with the protein chain [24–26].

Despite the low sequence identity (Fig. 1), the structures of plastidic- and bacterial-type FNRs indicate that they share some common structural and functional characteristics. They all display a two domain arrangement ($NADP^+$- and FAD-binding domains) and are highly specific towards NADPH *versus* NADH [15,27–31]. Moreover, they share six conserved peptide segments involved in FAD- or NADP(H)-binding and the position of the flavin is held at the interface between the two structural domains, being the isoalloxazine moiety stacked at its *si*-face by a conserved aromatic residue (Tyr79 in *Anabaena* FNR and Tyr66 in *Rhodobacter capsulatus* FPR (*Rc*FPR)). However, the structural analysis also reveals specific structural features of each group that could be associated to their different catalytic function, turnover, reaction direction and protein partner. In particular, the conformation of the FAD cofactor is open in plastidic FNRs but bended in bacterial FPRs [15,30–32]. Besides, bacterial enzymes carry an extended C-terminus when compared with plastidic ones, while the later ones invariantly end at a C-terminal Tyr that stacks against the *re*-face of the isoalloxazine. The C-terminal extension present in bacteria FPRs is involved in NADP(H) efficient binding, allowing affinity levels compatible to catalysis [2,33]. FPRs can be further classified in two groups depending on the nature of the aminoacid located at the *re*-face of the isoalloxazine at the position of the C-terminal Tyr in plastidic FNRs, which can be aliphatic (subclass I) as in *Rc*FPR, or aromatic (subclass II) as in *Escherichia coli* FPR [2].

Mutational analysis, fast kinetic methods and experimental and computational structural approaches have been thoroughly used to characterise coenzyme binding and HT for plastidic FNRs [12,19–21,24,34,35]. The nicotinamide moiety of the coenzyme (NMN) approaches the isoalloxazine ring on its *re*-face, while the C-terminal Tyr side-chain is proposed to get slightly displaced letting the rings to stack. However, it is proposed to remain in the catalytic site preventing the formation of a strong [isoalloxazine-H]$^-$:$NADP^+$ close contact ionic pair, a fact related with the forward (photosynthetic) and the backward (non-photosynthetic) HT reactions taking place with similar rate constants in these enzymes [21,36]. The occurrence of charge transfer complexes (CTC) and similar HT rates observed for *Rc*FPR, suggested that an equivalent

```
Consensus                     Rx YS                          Yxx          G xxS             GTGIxP

Anabaena sp.       ---KPEKLRL YSIASTRHGD DVDDKTISLC VRQLEYKHPE SGET---VYG VCSTYLTHIE ··· ATGTGIAPMR ···
Synechococcus sp.  ---KPHKLRL YSIASTRHGD MEDNKTVSLC VRQLEYQDPE SGET---VYG VCSTYLCNLP ··· ATGTGIAPFR ···
Synechocystis sp.  ---KPHKLRL YSIASTRHGD FGDDKTVSLC VRQLEYQN-E AGET---VQG VCSTYLCNIK ··· ATGTGIAPFR ···
Spirulina sp.      ---KPHKLRL YSIASTRHGD HVDDKTVSLC VRQLEYKHPE TGET---VYG VCSTYLCNLE ··· ATGTGIAPFR ···
S. oleracea leaf   ---KPHKLRL YSIASSALGD FGDAKSVSLC VKRLIYTN-D AGET---IKG VCSNFLCDLK ··· GTGTGIAPFR ···
O. sativa leaf     ---KPHKLRL YSIASSALGD FGDSKTVSLC VKRLVYTN-D QGEI---VKG VCSNFLCDLK ··· ATGTGIAPFR ···
P. sativum leaf    ---KPHKLRL YSIASSAIGD FGDSKTVSLC VKRLVYTN-D AGEV---VKG VCSNFLCDLK ··· GTGTGIAPFR ···
N. tabacum leaf    ---KPHKLRL YSTASSALGD FGDSKTVSLC VKRLVYTN-D KGEE---VKG VCSNFLCDLK ··· ATGTGIAPFR ···
A. thaliana leaf   ---KPHKLRL YSIASSAIGD FGDSKTVSLC VKRLVYTN-D GGEI---VKG VCSNFLCDLK ··· GTGTGIAPFR ···
O. sativa root     ---APHNVRL YSIASTRYGD SFDGRTTSLC VRRAVYYDPE TGKEDPSKNG VCSNFLCNSK ··· ATGTGVAPFR ···
P. sativum root    ---SPHNVRL YSIASTRYGD NFDGKTASLC VRRAVYYDPV TGKEDPSKNG VCSNFLCDSK ··· ATGTGVAPYR ···
N. tabacum root    ---NPHNVRL YLIASTRYGD SFDGKTASLC VRRAVYYDPE TGKEDPSKNG VCSNFLCDSK ··· GTGTGVAPFR ···
A. thaliana root   ---APHNVRL YSIASTRYGD SFDGKTASLC VRRAIYYDPE TGKEDPSKAG VCSNFLCNAK ··· ATGTGVAPYR ···
L. interrogans     LADVGYTVRL YSIASPSYSF GMKEDNIEFI IKRDNIYDEN GNIQ---FKG VCSNYMCDLK ··· ATGTGIAPFI ···
A. vinelandii      ---GRPLMRA YSIASPNYEE HLEFFSIKVQ N--------- ---------G PLTSRLQHLK ··· STGTGLAPFM ···
P. aeruginosa      ---GRPLMRA YSIASPNYEE HLEFFSIKVP D--------- ---------G PLTSRLQHLK ··· STGTGMAPFL ···
X. axonopodis      ---TRPLLRA YSIASANWEE HLEFFSIKVP D--------- ---------G PLTSRLQHIQ ··· GTGTGLAPWL ···
R. capsulatus      ---GKPIMRA YSIASPAWDE ELEFYSIKVP D--------- ---------G PLTSRLQHIK ··· ATGTGIAPFA ···
A. vinelandii      -ADGGTVWRA YSMVSAPADD YLEFFSVVVP G--------- ---------G EFTSELCRLG ··· ATGTGLGPFL ···
E. coli            --DGERVQRA YSYVNSPDNP DLEFYLVTVP D--------- ---------G KLSPRLAALK ··· ATGTAIGPYL ···
B. aphidicola APS  PLNKNKIQRA YSYVNAPSEK NLEIYIVRVL N--------- ---------G QLSNLLYNLH ··· ATGTGIGPYC ···

Consensus                 SR          YxCGL                                         ExY

Anabaena sp.       RLTYAISRE- ··· KTHTYICGLR GMEEGIDAAL SAAAAKEGVT WSDYQKDLKK AGRWHVETY
Synechococcus sp.  RLTYAISRE- ··· NTHVYMCGLK GMQPPIDETF TAEAEKRGLN WEEMRRSMKK EHRWHVEVY
Synechocystis sp.  RLTLAISRE- ··· KTHTYMCGLK GMEPGIDEAF TALAEQNGKE WTTFQREMKK EHRWHVETY
Spirulina sp.      RLDFAVSRE- ··· NTHTYICGLK GMEGGIDEGM SAAAGKFDVD WSDYQKELKK KHRWHVETY
S. oleracea leaf   RVDYAVSRE- ··· NTYFYMCGLK GMEKGIDDIM VSLAAAEGID WIEYKRQLKK AEQWNVEVY
O. sativa leaf     RLDFAVSRE- ··· HTYVYMCGLK GMEKGIDDIM VSLAAKDGID WADYKKQLKK GEQWNVEVY
P. sativum leaf    RLDFAVSRE- ··· NTFVYMCGLK GMEKGIDDIM VSLAAKDGID WIEYKRTLKK AEQWNVEVY
N. tabacum leaf    RLDFAVSRE- ··· NTFIYMCGLK GMEQGIDEIM SALAERDGIV WADYKKQLKK AEQWNVEVY
A. thaliana leaf1  RLDFAVSRE- ··· NTFVYMCGLK GMEKGIDDIM VSLAAKDGID WLEYKKQLKR SEQWNVEVY
O. sativa root     RYDKALSRE- ··· -AHIYFCGLK GMMPGIQDTL KKVAEQRGES WEQKLSQLKK NKQWHVEVY
P. sativum root    RYNRALSRE- ··· -AHIYFCGLR GMMPGIQETL KRVAEKRGES WEEKLSQLKK NKQWHVEVY
N. tabacum root    RYDRALSRE- ··· -AHIYFCGLK GMMPGIQDTL KRVAERRGES WEQKLSQLKK NKQWHVEVY
A. thaliana root1  RYDKALSRE- ··· -AHIYFCGLK GMMPGIQDTL KRVAEERGES WEQKLTQLRK NKQWHVEVY
L. interrogans     KLITAISREE ··· GRFYICGGPK GMEKGVIEEI QKISGNTG-T YEEFKHHLEG AHQLFVETY
A. vinelandii      IYYPTVTRES ··· DDRAMICGSP SMLDESCEVL DGFGLK---- ---ISPRMGE PGDYLIERAFVEK--
P. aeruginosa      IYYPLVTREP ··· DDRAMICGSP SMLEETSAVL DSFGLK---- ---ISPRMGE PGDYLIERAFVEK--
X. axonopodis      LYYPAVTRET ··· NDRFMICGSP QMLADLRSLL DSRGFQ---- ---TSPRIGT PGHYVFERAFVEK--
R. capsulatus      KYYPTTTREE ··· TDRAMVCGSL AFNVDVMKVL ESYGLR---- ---EGANS-E PREFVVEKAFVGEGI
A. vinelandii      QYLPLVTREA ··· CSRLMLCGNP QMIKDCRELL K-ARGL---- ---QLSLSRK PGQVAVENYW-----
E. coli            RIQTVVSRET ··· TSHVMLCGNP QMVRDTQQLL KETRQM---- ---TKHLRRR PGHMTAEHYW-----
B. aphidicola APS  QIQTITSREK ··· TSHVMLCGNP FMVKDTFLFL KNNRNM---- ---EKHLRRK KGHITMENYW-----
```

Fig. 1. Sequence alignments of plant-type FNRs. Conserved regions in plant-type FNRs, regardless of their plastidic or bacterial origin are shaded in purple, and their consensus sequences showed in bold. Plastidic-type characteristic aminoacids interacting with the FAD adenosine are shaded in green.

mechanism may be happening in bacterial homologues [33]. Moreover, structural analysis of the *Rc*FPR:$NADP^+$ crystallised complexes reveals that the six-residue C-terminal tail present in *Rc*FPR might be displaced to allow entrance of the NMN in the catalytic cavity. In addition, this movement could modulate nicotinamide occupancy, analogously to the C-terminal Tyr in plastidic enzymes [20,33].

To explore the involvement of the C-terminal extension occurring in the bacterial subclass I FPR in nucleotide binding and HT, we generated a series of mutants in *Rc*FPR either lacking the aminoacid extension beyond Ala266 and/or replacing this residue by a Tyr; namely A266Y, A266-$\Delta_{267–272}$ and A266Y-$\Delta_{267–272}$. Biochemical and structural analysis of the mutants provides some clues about the contribution of the C-terminal extension to the oxido-reduction properties of the flavin, the coenzyme allocation in the catalytic competent organization, the HT process and the general stability of these bacterial flavoenzymes.

2. Materials and methods

2.1. Expression vector design, protein expression and purification

To obtain the deletion mutants at the C-terminal extension of *Rc*FPR, the WT coding sequence in the plasmid pGEM-fpr-*Nco* [14] was amplified using oligonucleotide 5′-ATTgCCATggCgAAAgTCCTgC-3′ as forward primer, and 5′-TCAggCCTTTTCCACCACgAA-3′, 5′-TCAgATgCCTTCgCCgA CgAAgTACTTTTCCACCACg-3, 5′-TCAggCCTTTTCCACCACgAA-3′, and 5′-gTCAATACTTTTCCACCACGAATTCg-3′ as reverse primers for WT, A266Y, A266-$\Delta_{267–272}$ and A266Y-$\Delta_{267–272}$ respectively. The products of the PCR amplifications were introduced into the pGEM®-T easy vector, using the ligation mixture to transform *E. coli* DH5α. After plasmid DNA isolation from transformed cells, the *Nco*I–*Sac*I fragment of each clone was ligated into compatible sites of the expression vector pET-32a that allows expression of recombinant proteins as tioredoxin-His_6 fusion, easily purified trough Ni-NTA (Quiagen) affinity chromatography. Mutations were verified by DNA sequence analysis after amplification in the same strain. *Rc*FPR variants were overexpressed in *E. coli* BL21(DE3) pLys transformants after induction with 0.50 mM IPTG at 20 °C for 16 h, purified trough affinity chromatography and subsequently dialysed against 50 mM Tris–HCl pH 8.0. The fusion proteins were finally digested with enterokinase and the released tioredoxin-His_6 tag was removed by Q-Sepharose chromatography procedure.

2.2. Spectroscopic and fluorescence measurements

Absorption spectra were recorded on a Shimadzu UV-2450 spectrophotometer. Titrations of *Rc*FPR_{ox} with $NADP^+$ were performed spectrophotometrically at 25 °C. The enzyme was diluted to a final concentration between 20 and 70 μM in 50 mM Tris–HCl, pH 8.0. Difference spectra were computed by subtracting from each spectrum the one obtained in the absence of ligand, after correction for dilution. Dissociation constants (K_d) were calculated by fitting data sets to the equation of a rectangular hyperbole using SigmaPlot (Systat Software Inc., Point Richmond, CA). The estimated error in the measured parameters is ±15% in K_d, and ±5% in $\Delta\varepsilon_{max}$. Phototitrations were performed at 10 °C in 50 mM Tris–HCl, pH 8.0, under anaerobic conditions. The spectrophotometer cell contained 20 μM *Rc*FPR, 3 mM EDTA and 2 μM 5-deazariboflavin. Stepwise reduction of the *Rc*FPR variants was achieved by light irradiation from a 250 W slide projector for different periods of time, and the UV–vis spectrum was then recorded in a Cary 100 spectrophotometer.

The flavin fluorescence was monitored using a Varian Cary Eclipse fluorescence spectrophotometer interfaced with a personal computer. The solution for fluorescence measurements contained 3 μM proteins in 50 mM Tris–HCl pH 8.0. The samples were previously filtered through a desalting column. FAD fluorescence (λ_{exc} = 445 nm; λ_{em} = 500–600 nm) was registered both before and after the addition of increasing concentrations of $NADP^+$ at 25 °C. To determine K_d for binding of nucleotide to the enzyme, maximum emission data were fitted to the equation of a rectangular hyperbole using SigmaPlot (Systat Software Inc., Point Richmond, CA) and estimated with an error of ±15%. Quenching of flavin fluorescence by iodine was used to investigate the relative accessibility of FAD in the *Rc*FPR WT and mutants [37]. The emission fluorescence at 525 nm (λ of emission 445 nm) of a 2 mL sample of *Rc*FPR in 50 mM Tris–HCl, pH 8.0 was determined during the titration of KI in cuvettes with a 1-cm pathlength at 25 °C. The samples were previously filtered through a sephadex G25 column to remove free FAD.

2.3. ThermoFAD experimental setup

Experiments were performed using a real-time PCR detection system with 96-well RT-PCR plates (Mastercycler® ep realplex^2, Eppendorf). Measurements were performed using an excitation wavelength range between 470 and 500 nm and a SYBR Green fluorescence emission filter (523–543 nm) which overlaps the fluorescence spectrum of the isoalloxazine ring (470–570 nm) [38]. The flavoprotein concentration required for optimal signal-to-noise ratio was initially evaluated using WT *Rc*FPR as a benchmark. Unfolding curves were generated using a temperature gradient from 20 to 85 °C, performing a fluorescence measurement after every 1 °C increase. All experiments were performed at least three times, and the reported T_m values are based on the mean values determined from the peaks of the derivatives of the experimental data. The best concentrations for ThermoFAD analysis were between 0.5 and 1 mg/mL in a final volume of 20 μL in 50 mM Tris–HCl, pH 8.0, and all subsequent experiments were carried out using protein concentrations in this range.

2.4. Isothermal titration calorimetry (ITC)

ITC experiments were conducted using a high precision VP-ITC system (MicroCal LLC, Northampton, MA). Buffered solutions of *Rc*FPR variants (2–15 μM) were titrated with $NADP^+$ (40–450 μM) prepared in the same buffer. Measurements were carried out in 50 mM Tris–HCl and 50 mM and MOPS, both at pH 8.0, two buffers with different ionisation enthalpies: MOPS, 5.05 kcal/mol and Tris–HCl, 11.35 kcal/mol [39]. Each titration experiment was initiated by a 4 μL injection (not used in the final data analysis), followed by 28 stepwise injections of 10 μL. The binding enthalpy (ΔH), the association constant (K_a), and the stoichiometry of the binding were obtained through least-squares non-linear regression of the experimental data to a model for one binding site implemented in Origin 7.0 (OriginLab). The determined K_a does not contain any buffer contribution as long as the pH of the experiment is close enough to the pK_a of the employed buffer. The buffer-independent binding enthalpy, ΔH^0, can be obtained by eliminating the contribution of the buffer ionisation, ΔH_{ion}, from the observed binding enthalpy, ΔH, according to: $\Delta H = \Delta H^0 + n_{H+}\Delta H_{ion}$, being n_{H+} the net number of protons exchanged between the complex and the bulk solution [40]. The free energy change (ΔG) and the entropy change (ΔS) were obtained from basic thermodynamic relationships. The estimated error in the measured parameters is ±15% in K_a and K_d, ±2–5% in ΔG, and ±5–10% in ΔH and −TΔS.

2.5. Steady-state kinetic analysis

Diaphorase activities were measured at 25 °C in reaction mixtures containing 50 mM Tris–HCl, pH 7.2, 3 mM glucose 6-phosphate, 0.6 mM $NADP^+$, 1 unit of glucose-6-phosphate dehydrogenase, and either 100 μM 2,6-dichlorophenolindophenol (DCPIP) or 1 mM $K_3Fe(CN)_6$ as electron acceptor [20]. After the addition of 20 nM enzyme, the reactions were monitored spectrophotometrically by following substrate reduction at 420 nm for $K_3Fe(CN)_6$ (ε_{420} = 1 mM^{-1} cm^{-1}) or at 600 nm (ε_{600} = 21 mM^{-1} cm^{-1}) for DCPIP. For the estimation of kinetic parameters of the diaphorase reaction, measurements were carried out at different NADPH concentrations, at a fixed saturating concentration of $K_3Fe(CN)_6$ or DCPIP. Steady state data were fitted to the theoretical curves using SigmaPlot (Systat Software Inc., Point Richmond, CA). The estimated error in the measured parameters is ±10–15% in K_m, and ±5–10% in k_{cat}.

2.6. Stopped-flow pre-steady-state kinetic measurements

Reduction of A266Y, A266-$\Delta_{267–272}$ and A266Y-$\Delta_{267–272}$ *Rc*FPR$_{ox}$ by NADPH was analysed by stopped-flow in 50 mM Tris–HCl, pH 8.0 at 25 °C under anaerobic conditions. The final *Rc*FPR concentration was 8 μM, while an 8–250 μM range was used for the nucleotide. Reactions were analysed by following the evolution of the absorption spectra (400–1000 mm) using an Applied Photophysics SX17.MV stopped-flow and a photodiode array detector. Multiple wavelength absorption data were collected and processed using the X-Scan software (Applied Photophysics Ltd.). The instrument dead time was 2–3 ms under these conditions. Time spectral deconvolution was performed using Pro-Kineticist (Applied Photophysics Ltd.) by data fitting to a two step, A → B → C, model, allowing estimation of the observed conversion rate constants (k_{obs}: $k_{A\rightarrow B}$, $k_{B\rightarrow C}$) [36]. A, B and C are spectral species, reflecting a distribution of enzyme intermediates (reactants, CTCs, Michaelis-complexes, products) at a certain point along the reaction time course, and do not necessarily represent a single distinct enzyme intermediate. Model validity was assessed by lack of systematic deviations from residual plots at different wavelengths, inspection of calculated spectra and consistence among the number of significant singular values with the fitted model. k_{obs} showed a saturation profile on the NADPH concentration that fit to the equation

$$k_{obs} = \frac{k_{HT}[\mathrm{NADPH}]}{[\mathrm{NADPH}] + K_d}$$

and allowed determination of K_d^{NADPH} as well as the HT rate constant, k_{HT} [36]. The estimated error in the measured parameters is ±15% in K_d^{NADPH}, and ±10% in k_{HT}.

2.7. Crystal growth, data collection and structure refinement

Crystals of the A266Y-$\Delta_{267–272}$ *Rc*FPR mutant were grown at 18 °C using the hanging-drop vapour diffusion method by mixing 1 μL protein solution containing 50 mM Tris–HCl, pH 8.0, 50 mM NaCl and 20 mM $NADP^+$ with 1 μL of crystallisation buffer containing 100 mM BIS–Tris–HCl, pH 5.5 and 21% (wt/vol) PEG 3350. The best crystals were grown with protein at 8 mg/mL. They belong to the trigonal $P3_121$ space group and display the following unit cell dimensions: a = b = 74.96 Å, c = 188.62 Å. Crystals were cryo-protected by the crystallisation buffer with a supersaturated solution of sodium acetate and frozen in liquid nitrogen. Diffraction data were collected at the ESRF (Experimental *Synchrotron* Research Facility at Grenoble, France) beamline ID14-4 to the resolution of 1.7 Å. Data were processed using iMOSFLM [41] and SCALA [42] programmes from the CCP4 package [43]. The data statistics are summarised in Table SP1. The structure was solved by molecular replacement using the MOLREP programme [44] with the native *Rc*FPR structure (PDB code 2bgi) as the first search model. A unique and unambiguous solution for the rotation and translation functions was obtained. There are two A266Y-$\Delta_{267–272}$ *Rc*FPR molecules in the asymmetric unit of the crystal. Phases calculated from the initial solution were subjected to alternated cycles of refinement with PHENIX programme [45] and manual model building with COOT [46]. The good quality of the final electron density maps allowed us to model 251 aminoacids for the polypeptide chain (residues 16–266 in chains A and B). One FAD was found bound to each *Rc*FPR molecule and, also, one sulphate ion in molecule A. The quality of the final geometry was checked with PROCHECK [47]. The final model has a R_{work}/R_{free} of 17.7%/19.5%. The refinement statistics are summarised in Table SP1. Atomic coordinates and structure factors are deposited in the PDB with the accession code: 4K1X.

3. Results

3.1. Spectroscopic characterisation of the RcFPR variants

The A266Y, A266-$\Delta_{267–272}$ and A266Y-$\Delta_{267–272}$ *Rc*FPR mutants were isolated as recombinant fusion proteins from cleared extracts of *E. coli* transformants which rendered similar yields than the WT enzyme after affinity chromatography purification and removal of the fused tioredoxin-His_6 tag. Their UV–vis spectral shape resembled that of WT *Rc*FPR, although maxima positions of the flavin absorbance bands resulted slightly displaced to larger wavelengths (Fig. 2A, Table SP2). Extinction coefficients of the flavin absorption peak at 450 nm (band-I) determined by protein denaturation and FAD release, for WT ($\varepsilon = 11.7$ mM^{-1} cm^{-1}) and A266-$\Delta_{267–272}$ *Rc*FPRs ($\varepsilon = 11.3$ mM^{-1} cm^{-1}) resulted similar to that of the free FAD ($\varepsilon = 11.5$ mM^{-1} cm^{-1}), indicating that the protein environment barely affects this parameter. Replacement of Ala266 with a Tyr caused a decrease of extinction coefficients ($\varepsilon = 10.12$ mM^{-1} cm^{-1} for A266Y and $\varepsilon = 9.73$ mM^{-1} cm^{-1} for A266Y-$\Delta_{267–272}$) to values similar to those occurring in plastidic FNRs ($\varepsilon = 9.4$ mM^{-1} cm^{-1} for *Anabaena* FNR), where a highly conserved Tyr stacks against the *re*-face of the isoalloxazine.

Emission spectra of FAD in the *Rc*FPR variants resulted in the maxima generally displaced 7–12 nm to higher wavelengths with respect to the WT (Fig. 2B, Table SP3), particularly when Ala266 is replaced by Tyr. However, this substitution only caused subtle changes in the relative intrinsic fluorescence of the bound flavin, whereas deletion of the 267–272 tail led to a 6-fold increase of this parameter and the simultaneous replacement of Ala266 to Tyr again reduced it. This later effect is probably due to quenching phenomena caused by the presence of the aromatic side-chain. These results also suggest a greater exposure of the isoalloxazine ring towards the solvent in the deletion mutants. This hypothesis was further confirmed by the addition of iodine as fluorescence quencher that allows quantification of the accessibility of the triple ring. For WT *Rc*FPR the exposure of the isoalloxazine was evaluated as 40% of the free FAD, while a value near 100% was obtained for all three studied variants. The augmented exposure of the cofactor towards the solvent implies a relaxation of the protein environment that can be visualised following the ThermoFAD protocol [38]. This procedure allowed the surveillance of the FAD fluorescence during a thermal denaturing process revealing decreases of 16.5 °C, 12 °C and 10.5 °C in the T_m of the A266-$\Delta_{267–272}$, A266Y-$\Delta_{267–272}$ and A266Y mutants when compared to the WT *Rc*FPR (Fig. 2C).

All *Rc*FPR variants resulted efficiently photoreduced (Fig. 2D and E), but the process showed important differences regarding stabilisation of the neutral semiquinone described for the WT (characterised by an absorbance maximum at 600 nm) [33]. No semiquinone stabilisation at all was observed for the A266Y variant and very little was detected for A266Y-$\Delta_{267–272}$ *Rc*FPR. A266-$\Delta_{267–272}$ *Rc*FPR suffered several spectral band displacements, including the intermediate stabilisation of a broad band centred at ~550 nm and the displacement of the band II of the flavin up to 340 nm. Such observations might be compatible with the transient stabilisation of traces of an anionic semiquinone along the photoreduction of this variant [48].

3.2. Binding of the coenzyme to the RcFPR variants

Difference spectra of the *Rc*FPR:$NADP^+$ complexes were obtained to investigate the relative architecture of the reacting isoalloxazine and nicotinamide rings. $NADP^+$ binding to the WT *Rc*FPR produced a difference spectrum characterised by a band at 505 nm and a valley around 434 nm [33]. Both of these features are also observed for the interaction of chloroplastic FNRs (but not cyanobacterial), and have been related to

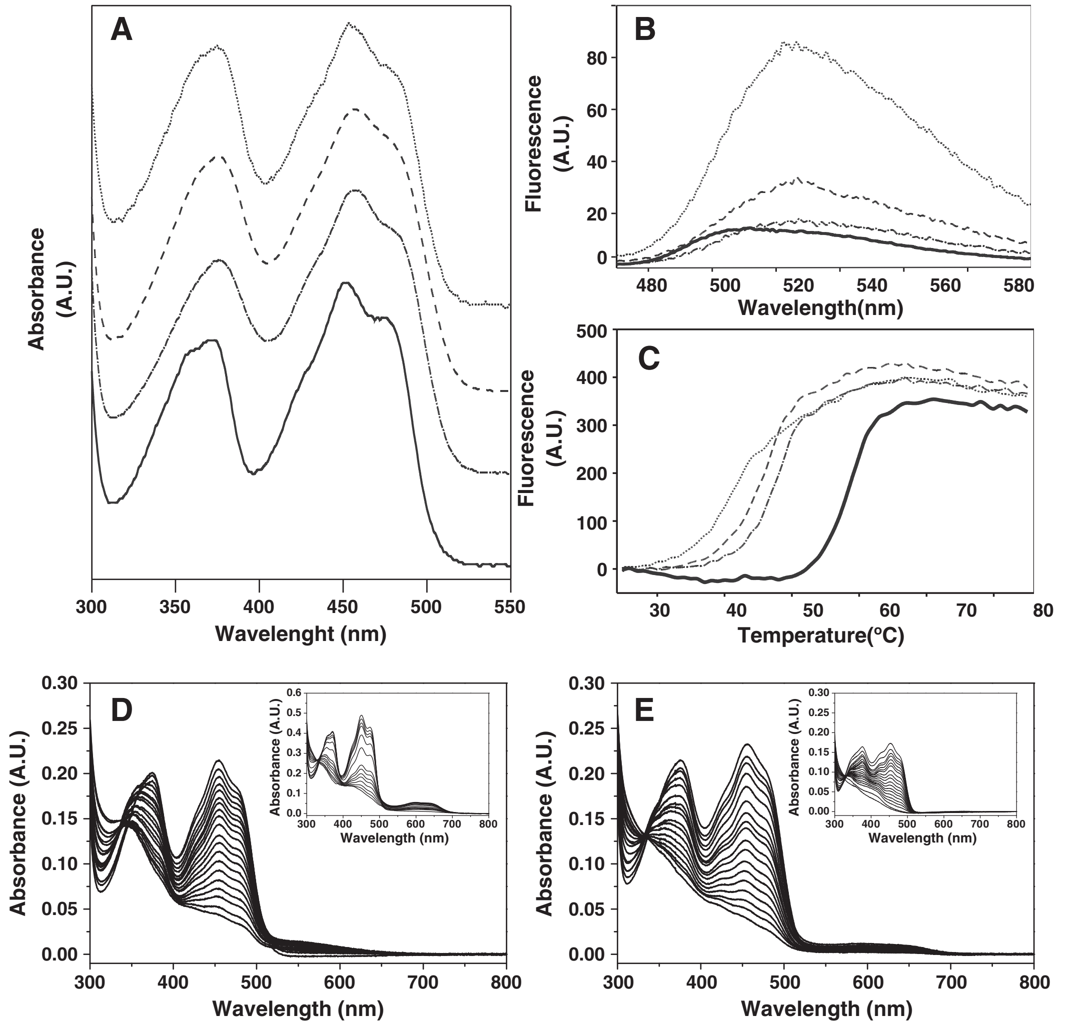

Fig. 2. Spectroscopic characterisation of the *Rc*FPR variants. (A) UV visible absorption spectra, (B) fluorescence emission spectra and (C) thermogram for the denaturation followed by FAD liberation of WT (solid line), A266Y (dashed–dotted line), A266-$\Delta_{267-272}$ (dotted line) and A266Y-$\Delta_{267-272}$ (dashed line) *Rc*FPR. Absorbance spectra obtained along photoreduction of (D) A266-$\Delta_{267-272}$ *Rc*FPR (WT in the inset) and (E) A266Y-$\Delta_{267-272}$ *Rc*FPR (A266Y in the inset). All photoreduction measurements were recorded using 20 μM flavoenzyme in 50 mM Tris–HCl, pH 8.0 at 25 °C.

an optimized geometry of the isoalloxazine:nicotinamide interaction ready for HT [12,20]. Difference spectra obtained for the variants under similar conditions showed displacement to longer wavelengths and reduction in intensity of the 505 nm band, while the valley also shifted towards ~450 nm, suggesting modification of the isoalloxazine environment upon coenzyme binding with respect to WT. Saturation of the difference spectra upon increasing $NADP^+$ concentration allowed determination of K_d^{NADP+} as well as of the magnitude of the spectroscopic change, Δε (Table 1). The affinity for $NADP^+$ considerably increased for all *Rc*FPR variants with respect to the WT, particularly for A266Y-$\Delta_{267-272}$ (up to 35-fold). However, Δε in the ~505 nm band, reflecting the occupancy of the nicotinamide into the flavin environment, decreased up to 2-fold in the A266-$\Delta_{267-272}$ and A266Y-$\Delta_{267-272}$ *Rc*FPRs and up to 6-fold for A266Y *Rc*FPR. Binding of $NADP^+$ to WT *Rc*FPR produces a raise on the fluorescence intensity that has been related to a greater exposure of the flavin isoalloxazine ring upon nicotinamide location at the active site. Changes in fluorescence showed also a saturation profile for all variants that enables determination of K_d^{NADP+} (Table 1) in agreement with those obtained by difference spectroscopy. Fluorescence increase upon $NADP^+$ binding by the mutated species was always lower than the corresponding to WT *Rc*FPR.

Coenzyme binding analysis based on flavin absorbance or fluorescence, mainly sense changes in the isoalloxazine environment forced by coenzyme location in the flavoprotein, and particularly by the final geometry of nicotinamide:isoalloxazine species. Calorimetric measurements also allow estimation of overall complex formation parameters independently of the sticking at the isoalloxazine environment. Analysis

Table 1
Interaction parameters for the binding of $NADP^+$ to the different *Rc*FPR variants.

	Differential spectroscopy[a]		Fluorescence[b]		
	K_d (μM)	λ_{max} (nm)	$\Delta\varepsilon_{max}$ (mM^{-1} cm^{-1})		K_d (μM)
WT	222	505	0.31		215
A266-$\Delta_{267-272}$	10.0	520	0.14		7.0
A266Y	14.1	515	0.06		16
A266Y-$\Delta_{267-272}$	6.0	518	0.16		4.0
	Isothermal titration calorimetry[c]				
	K_d (μM)	ΔG° (kcal/mol)	ΔH° (kcal/mol)	−TΔS° (kcal/mol)	n_{H+}
WT	66	−5.7	−2.6	−3.1	0.11
A266-$\Delta_{267-272}$	2.0	−7.8	−8.0	+0.2	−1.03
A266Y	0.87	−8.3	+2.4	−10.7	−0.24
A266Y-$\Delta_{267-272}$	4.4	−7.3	−5.8	−1.5	−0.48

[a] Data in 50 mM Tris–HCl, pH 8.0 at 25 °C.
[b] Data in 10 mM Tris–HCl, pH 8.0 at 25 °C.
[c] From measurements recorded in 50 mM Tris–HCl and in 50 mM MOPS both at pH 8.0.

by ITC of $NADP^+$ binding confirmed that all mutations significantly increased the affinity of *Rc*FPR for the nucleotide, and indicated that they considerably altered the enthalpic and entropic contributions to the binding process, particularly in the A266-$\Delta_{267–272}$ variant (Table 1, Fig. 3). In WT *Rc*FPR both enthalpic and entropic changes favourably contribute to coenzyme binding. Removal of the C-terminal tail in the A266-$\Delta_{267–272}$ mutant enhances the affinity for the coenzyme (30-fold), as a consequence of making the enthalpic contribution much more favourable than in the WT, though the entropy slightly opposes the interaction. The sole replacement of A266Y has a different effect displaying higher entropic contributions to the binding process, despite this variant also binds the coenzyme 75-times stronger than the WT. Finally, both enthalpic and entropic contributions also make more favourable the binding of the coenzyme to A266Y-$\Delta_{267–272}$ *Rc*FPR than in WT (Table 1, Fig. 3). Additionally, our data indicate that the WT and A266Y variants bind $NADP^+$ with negligible net proton exchange with the solvent, displaying a n_{H+} value near zero. However, the removal of the C-terminus in the deletion mutants shows that the coenzyme binding process is coupled to the release of one proton from the protein (Table 1).

3.3. Influence of the introduced mutations in the steady-state and pre-steady-state kinetic parameters of the HT from NADPH to RcFPR

The general decline of structure stability and the relaxation of the isoalloxazine protein environment produced by the mutations in the C-terminus had also important consequences on the enzymatic activity of *Rc*FPR (Table 2). All the *Rc*FPR variants suffered a 2- to 4-fold decrease of K_m^{NADPH} compared to the WT protein, in agreement with their higher affinities for $NADP^+$. However, catalytic rates were more dependent on the mutations. Substitution of Ala266 to Tyr led to a k_{cat} 3-fold lower than that of the native enzyme, while deletion of the C-terminal region resulted in *Rc*FPR variants which only maintained 5–10% of the original activity. The HT from NADPH to WT *Rc*FPR_{ox} was previously studied under anaerobic conditions using stopped-flow techniques with photodiode array detection [33]. The process fitted to a two step model

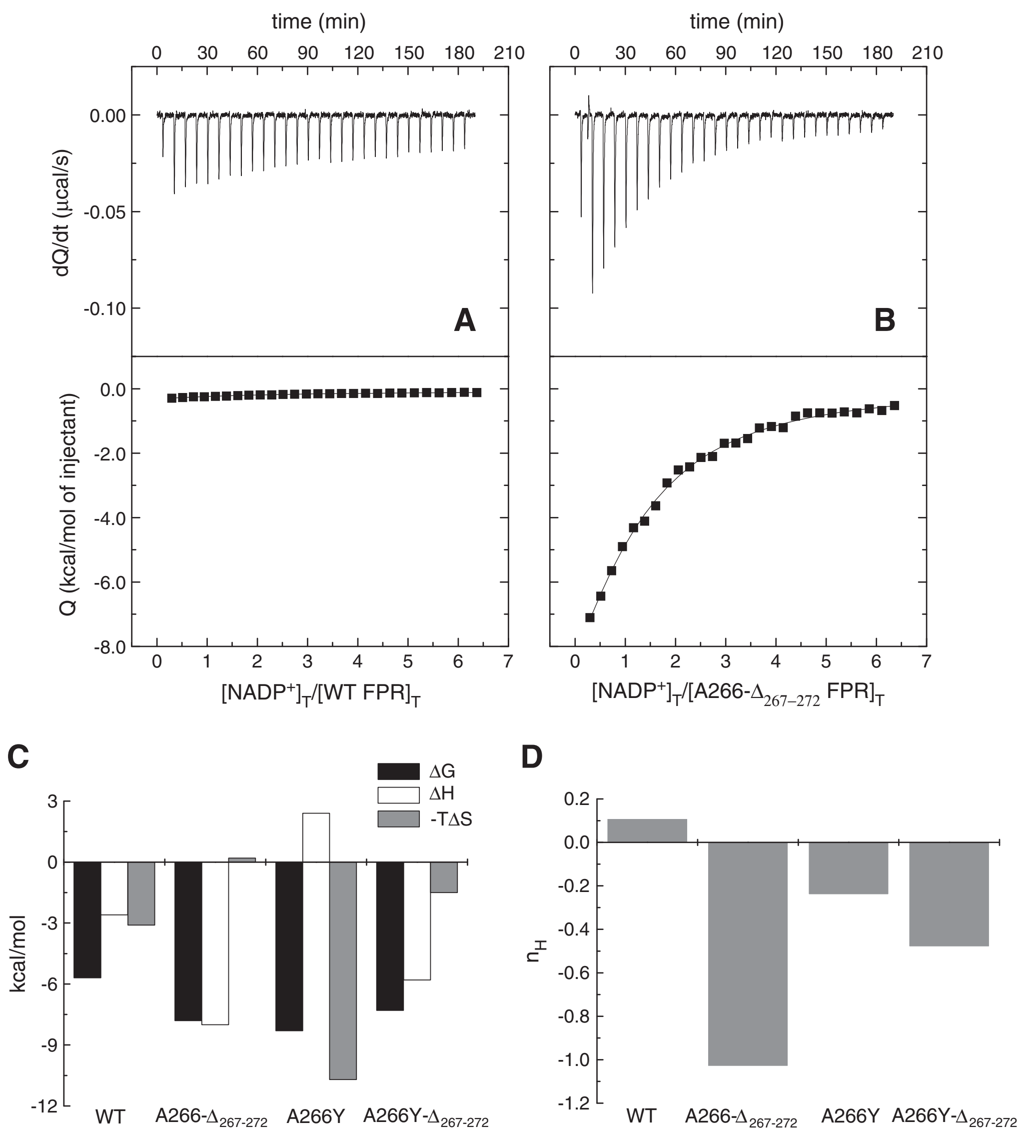

Fig. 3. Experimental calorimetric titrations of *Rc*FPR_{ox} variants with $NADP^+$. (A) Titration of WT *Rc*FPR (2 μM in the calorimetric cell) with $NADP^+$ (50 μM in the syringe) and (B) A266-$\Delta_{267–272}$ *Rc*FPR (15 μM) with $NADP^+$ (450 μM) in 50 mM Tris–HCl, pH 8.0, at 25 °C. Both the thermogram (top) and the binding isotherm (bottom) plots have been drawn at the same scale in both proteins for direct comparison. (C) Thermodynamic dissection of the binding interaction showing the Gibbs energy (black), enthalpy (white) and entropy (grey) of binding. (D) Net number of protons exchanged between the *Rc*FPR–$NADP^+$ complexes and the bulk solution.

Table 2
Steady-state and pre-steady-state kinetic parameters for the reduction of the different *Rc*FPR variants by NADPH.

	Steady-state				Pre-steady-state[c]	
	k_{cat} (s^{-1}) [a]	K_m^{NADPH} (μM) [a]	k_{cat} (s^{-1}) [b]	K_m^{NADPH} (μM)[b]	K_d^{NADPH} (μM^{-1})	k_{HT} (s^{-1})
WT	222	93	20	85	60.0	150.0
A266-$\Delta_{267–272}$	8	20	1	9	41.1	0.083
A266Y	68	32	7	43	25.0	126.6
A266Y-$\Delta_{267–272}$	12	43		39	31.7	0.058

[a] Data using $K_3Fe(CN)_6$ as substrate in 50 mM Tris–HCl, pH 7.2 and 25 °C.
[b] Data using DCPIP as substrate in 50 mM Tris–HCl pH, 7.2 and 25 °C.
[c] Data in 50 mM Tris–HCl, pH 8.0 and 25 °C.

A → B → C that evidenced this reaction taking place through the stabilisation of intermediate CTCs. Conversion of A into B was a very fast step that included certain reduction of the protein and the formation of an absorbance band centred at 560 nm that corresponds to a FAD: NADPH CTC, CTC-1. Species B evolved to a broad band centred at ~850 nm related to a $FADH^-$:$NADP^+$ CTC, CTC-2, and reached an equilibrium represented by species C. Upon HT from NADPH to the *Rc*FPR variants, none of them stabilised CTCs along the process, indicating that the geometry for the isoalloxazine:nicotinamide interaction during the HT process differs from that of WT (Fig. 4). All these HT processes fitted to an A → B → C model, but the main HT process was included in the first step and the second resulted in a much slower process of considerably less amplitude (Fig. 4). Spectral evolution of the deletion variants showed the appearance of a broad band extended towards 550 nm that might be related to a different CTC organisation. All, the WT and the mutated *Rc*FPRs, showed a saturation profile dependence of the observed rate for the main HT process on the NADPH concentration. Such behaviour allowed calculation of k_{HT} and K_d^{NADPH} (Table 2). The single substitution of Ala266 with Tyr had a minor effect on k_{HT}, but deletion of the 267–272 tail practically block HT. Regarding affinity for the reduced form of the coenzyme, all the variants showed a just mild increase.

3.4. Crystal structures

Conditions tested allowed crystallisation of the A266Y-$\Delta_{267–272}$ *Rc*FPR variant (see Mat & Met). Structure was solved by molecular replacement and refined up to 1.7 Å. The first 15 residues were not observed in the electron density map. Two molecules with similar conformation (r.m.s.d. of 0.67 Å for 251 Cα atoms) were present in the asymmetric unit and show an overall folding equivalent to the WT *Rc*FPR (r.m.s.d. for 251 Cα atoms of 0.95 and 1.13 Å for molecules A and B in the asymmetric unit, respectively). The main differences are concentrated in the $NADP^+$ domain, particularly in the Gly253–Glu257 loop and in the Leu173–Lys186 α helix, which appear displaced with respect to their positions in WT *Rc*FPR (Fig. 5A). The prosthetic group is found in a bent conformation in both molecules A and B (Fig. 5B and C), similar to the conformation adopted in the WT and in other bacterial FPRs [16]. This is a remarkable finding because the stabilisation of the FAD bent conformation present in WT *Rc*FPR was attributed to the extra 6-residue C-terminus tail (267–272), which has been removed in this mutant. In molecule A an extensive H-bond network, extended from the O2′ (ribityl) to O2A (pyrophosphate) via two water molecules (W25 and W217), seems to be the inducting force of the FAD bent conformation (Fig. 6A). However, no water molecules are present in this region of molecule B, and the FAD conformation is stabilised by Tyr266, as explained below (Fig. 6B). Other specific interactions between the apoprotein portion and FAD that are present in the WT also exist in the mutant, as the non-polar interaction between

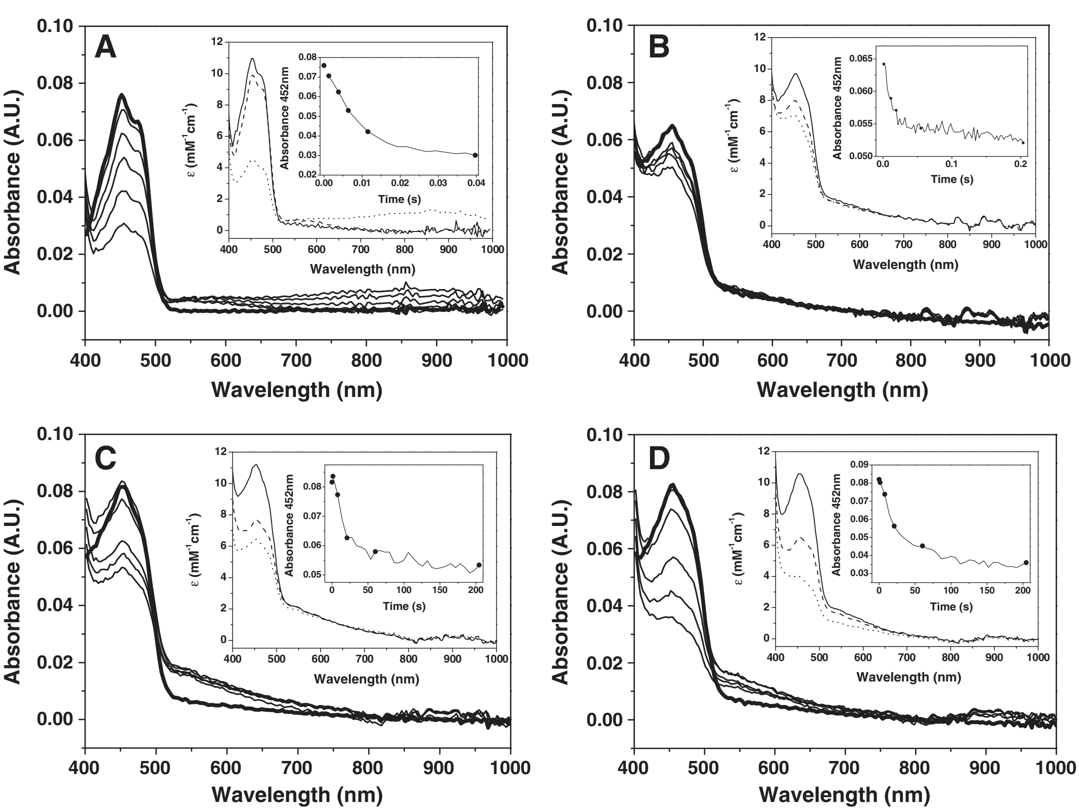

Fig. 4. Spectral evolution of the *Rc*FPR variants upon reduction by NADPH. Reduction with 150 μM NADPH of (A) 6.4 μM WT $RcFPR_{ox}$ (spectra recorded at 0.00128 s, 0.00384 s, 0.0064 s, 0.01152 s, and 0.03968 s after mixing), and with 80 μM NADPH of (B) 8 μM A266Y $RcFPR_{ox}$ (spectra recorded at 0.00128 s, 0.01152 s, 0.0192 s, 0.05504 s and 0.4928 s), (C) 8 μM A266-$\Delta_{267–272}$ $RcFPR_{ox}$ (spectra recorded at 1.309 s, 7.86 s, 20.97 s, 60.29 s and 204.5 s) and (D) 8 μM A266Y-$\Delta_{267–272}$ $RcFPR_{ox}$ (spectra recorded at 1.309 s, 7.86 s, 20.97 s, 60.29 s and 204.5 s). In all cases the thick line corresponds to $RcFPR_{ox}$ spectrum before mixing, the first inset shows the intermediate spectroscopic species after data fitting, and the second inset the absorbance evolution at 452 nm.

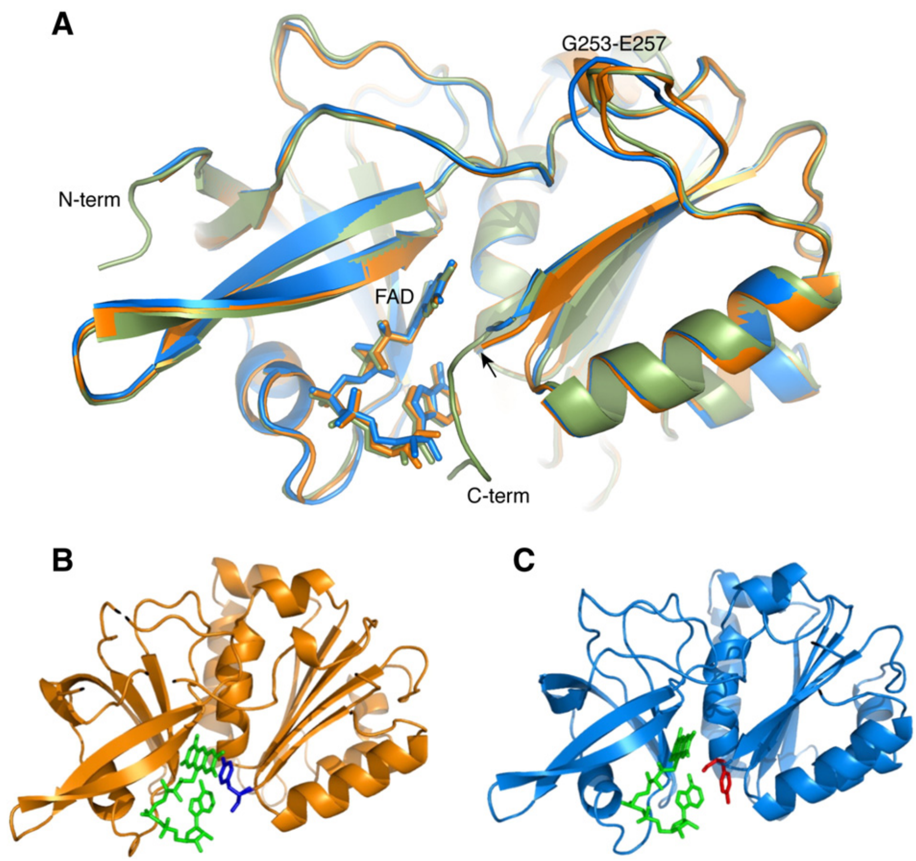

Fig. 5. Crystal structure of A266Y-$\Delta_{267-272}$ *Rc*FPR mutant. (A) Superposition of WT *Rc*FPR (green) (PDB code 2BGJ) and A266Y-$\Delta_{267-272}$ *Rc*FPR mutant (molecule A in orange and molecule B in blue). The N- and C-term regions in WT *Rc*FPR are labelled. The C-term end in the A266Y-$\Delta_{267-272}$ *Rc*FPR mutant is indicated by an arrow. The region Gly253 to Glu257 presenting some backbone differences among structures is labelled. (B) Cartoon representation of the molecule A of A266Y-$\Delta_{267-272}$ *Rc*FPR mutant. The FAD is shown as green sticks and Tyr266 as blue sticks. (C) Cartoon representation of the molecule B of A266Y-$\Delta_{267-272}$ *Rc*FPR mutant. The FAD is shown as green sticks and Tyr266 as red sticks. As observed in (B) and (C) the Tyr266 presents different conformation in the two molecules of the asymmetric unit of the A266Y-$\Delta_{267-272}$ *Rc*FPR crystal.

the adenosine and the hydrophobic Ile82 side-chain or the stacking between the isoalloxazine and Tyr66. Therefore, deletion of the 267–272 moiety does not significantly affect the conformation and stability of the FAD.

However, comparison of the two molecules of the asymmetric unit reveals remarkable differences in the allocation of the aromatic ring of Tyr266. While in chain A (Fig. 6A) the side-chain of the Tyr266 interacts with the isoalloxazine moiety of FAD (forming an angle of ~11.2°), in chain B (Fig. 6B) the stacking interaction takes place among the aromatic ring of the Tyr and the adenine group (forming an angle of ~23.2°). In this last molecule, N10 of the isoalloxazine is 3.1 Å from the main-chain carbonyl oxygen of Tyr266, an interaction that may help to stabilise the bent conformation of FAD (Fig. 6B). In addition, in molecule A (Fig. 6A), the phenolic -OH

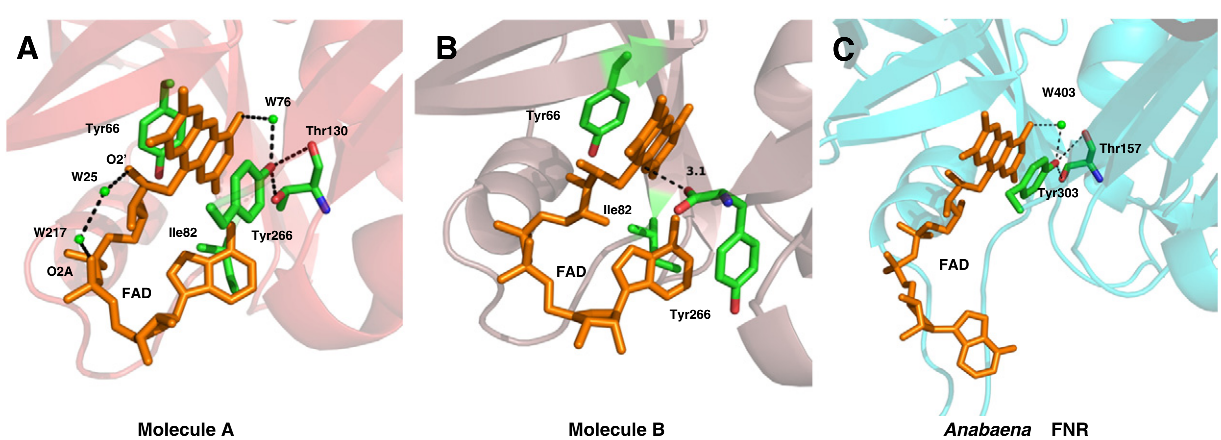

Fig. 6. The active site environment. Active sites of (A) Molecule A from A266Y-$\Delta_{267-272}$ *Rc*FPR, (B) Molecule B from A266-$\Delta_{267-272}$ *Rc*FPR and (C) FNR from *Anabaena* (PDB 1que). The FAD cofactor is coloured in orange. Residues involved in FAD binding are represented as sticks and by atom type (C, green; N, blue; O, red). The isolated green spheres represent water molecules.

group of Tyr266 is anchored though polar contacts with the -OH and C=O groups of Thr130, as well as with W76 (d[O(Tyr266)-OH(Thr130)] = 2.90 Å, d[O(Tyr266)-OH_2(W76)] =2.68 Å). Interestingly, similar interactions were observed in *Anabaena* FNR, where the Tyr303 hydroxyl group interacts with the hydroxyl of Thr157 and W403 located at the same position than Thr130 and W76 in the *Rc*FPR mutant (Fig. 6C).

4. Discussion

One of the most remarkable structural features of plastidic FNRs is the conservation of a C-terminal Tyr that stabilises the *re*-face of the isoalloxazine through π–π stacking, occupying the putative nicotinamide catalytic binding pocket in the free enzyme. Displacement of this residue upon coenzyme binding modulates the entrance of the nicotinamide of NADP(H) into the active site to attain a catalytic competent orientation while preventing formation of a strong stable ionic pair between both rings incompatible with an efficient turnover [21,34,49]. This Tyr additionally stabilises the flavin semiquinone and sets the midpoint potentials, therefore modulating the electron transfer rates towards the protein partners [20,25]. In bacterial FPRs the position of the plastidic C-terminal Tyr is replaced by a variable-length extension displaying two main features: i) one position ahead of the residue facing isoalloxazine there is an aromatic residue (Phe267 in *Rc*FPR) that stacks the adenine moiety of FAD which stabilizes its folded conformation, and ii) the residue facing the isoaloxazine, corresponding to the C-terminal Tyr in plastidic FNRs can be either aliphatic or aromatic, branching out the FPR group into subclass I (Ala266 in *Rc*FPR) and II, respectively [2]. The resolved crystal structure of *Rc*FPR suggested a particular importance for the C-terminal peptide starting at Ala266, AFVGEGI, in FAD stabilisation. Phe267 stacks the adenine moiety of FAD, whereas Val268, Gly271 and Ile272 establish a network of polar interactions with the ribityl and the ribose [15]. The C-terminal extension of bacterial FPRs is then proposed to displace allowing the nicotinamide to face the isoalloxazine ring [33], as it happens with the C-terminal Tyr in plastidic FNRs [7,15,21,33]. Rearrangement of residues located at the *re*-face of FAD appears to be required for efficient turnover in FPRs, while a restricted mobility of the C-terminal extension was envisaged as responsible for lower catalytic efficiency [2]. Therefore, similar roles to those of the C-terminal Tyr from plastidic FNRs might be expected for Ala266 and the C-terminal extension in *Rc*FPR inadjustment of substrate binding and flavin redox properties.

Following these hypotheses, three variants of *Rc*FPR have been produced here: the first one maintains the C-terminal extension, but Ala266 was replaced by a Tyr (A266Y); in the second the 267–272 extension was deleted (A266-$\Delta_{267-272}$); and finally, the third mutant is a combination of the previous two (A266Y-$\Delta_{267-272}$). Characterisation of these variants shows that the influence of the C-terminal extension on the catalytic event goes beyond previous considerations. Despite slight differences in absorbance/fluorescence maxima positions when compared to WT *Rc*FPR suggesting slight changes in the isoalloxazine environment, the three *Rc*FPR variants bind FAD without affecting the overall protein folding. Nevertheless, the absence of the C-terminal extension leads to a more solvent-exposed FAD (Fig. 2B and C), particularly in the A266-$\Delta_{267-272}$ variant. When a Tyr occupies position 266, extinction coefficients move to values similar to those of plastidic FNRs, indicating similar electronic properties of FAD. Actually, crystals obtained for the A266Y-$\Delta_{267-272}$ variant confirmed two configurations for Tyr266, only one of them facing the flavin ring (Fig. 6A and B). The stacked conformation of molecule A (Fig. 6A) might explain the decrease of intrinsic fluorescence regarding the A266-$\Delta_{267-272}$ variant (Fig. 2B), while a likely oscillation of Tyr266 in solution between the two positions illustrated in Fig. 6 would enable the high accessibility measured through quenching by iodine. Moreover, this plausible swing is consistent with the previously proposed movement of the WT C-terminal tail during $NADP^+$ entrance [33].

Binding of $NADP^+$ to WT *Rc*FPR is governed by the 2′P-AMP portion [33]. The three structures available for the *Rc*FPR:$NADP^+$ complex show binding of the nucleotide to the protein exclusively through its adenosine moiety, mainly through contacts with Arg158, Arg195 and Arg203 without directly involving the 266–272 region. Surprisingly, all the *Rc*FPR variants described here, particularly the deletion mutants, bind $NADP^+$ stronger than the WT, revealing that the C-terminal extension weakens coenzyme linkages after HT reaction. However, both variants introducing a Tyr at position of Ala266 increase affinity but decrease occupancy of the active site by nicotinamide (Table 1). In WT *Rc*FPR the C-terminal extension slightly narrows the preformed cavity to accommodate the 2′P-AMP portion of the coenzyme, where Arg158 H-bonds Ile272. This interaction results shifted upon $NADP^+$ binding, leading to the displacement of the C-terminal extension. Therefore, its removal might favour the initial binding of the 2′P-AMP moiety, as well as the subsequent allocation of the NMN moiety in the active site. However, difference spectra for the titration of A266-$\Delta_{267-272}$ with $NADP^+$ indicate a decreased nicotinamide occupancy in the active site as that for the WT, that is reflected by a diminished Δε at 505 nm (Table 1). All these data suggest a role for the C-terminal extension in alleviating the affinity for the oxidised form of the coenzyme.

Removal of the C-terminal extension had an important negative effect on the activity of *Rc*FPR. Despite affinity for the reduced form of the coenzyme resulted slightly increased in the shortened variants, calculated k_{cat} and k_{HT} values confirm that the HT from NADPH to the flavin is considerably hampered (Table 2). Additionally, HT processes occur with appearance of an altered CTC that reflects differences in the geometry of the FAD_{ox}:NADPH HT complex. The fact that HT rates drop up to 2000-fold for these two variants, while steady-state rates just suffered 10–20 fold decreases, might be related to the low stability of the reduced form of the flavoenzyme in the absence of the C-terminal extension. Such problem can be overcome during steady-state measurements by the presence of an acceptor that quickly recovers the oxidised enzyme. The single residue replacement occurring in the A266Y variant allows the formation of a complex compatible with HT, as shown by the k_{HT} and K_d^{NADPH} parameters being similar to the WT. Nevertheless, the lack of detection of a CTC during its reduction by NADPH confirms that the geometry of this HT complex is different than those of both the WT *Rc*FPR and the plastidic FNRs. Moreover, reduction of A266Y *Rc*FPR by NADPH only occurs to a very low extent, being the final spectral mixture displaced towards the oxidised enzyme form (Fig. 4). This displacement can be related to a non-optimal disposition of the reacting rings that could influence the midpoint potential of the mutant to more negative values than in WT [15]. Despite the low stability of the reduced mutants prevented determination of their midpoint reduction potentials, these observations and the decrease of stabilised semiquinone in the A266Y and A266-$\Delta_{267-272}$ variants during photoreduction suggest that Ala266 and the C-terminus structure contribute to modulate the oxido-reduction properties of *Rc*FPR (Fig. 2D and E).

ITC measurements during *Rc*FPR:$NADP^+$ complex formation also put on evidence the coupling of a proton release during coenzyme binding in the deletion mutants, revealing the presence of a proton acceptor to counterbalance the process in WT *Rc*FPR (Table 1). A conserved glutamate in the active site of FNRs (Glu312 in maize) is thought to function as proton donor/acceptor during catalysis, stabilising intermediate complexes through pK_a changes induced by binding of substrates [50]. This position corresponds to Glu264 in *Rc*FPR, recently proposed to undergo a pK_a decline after $NADP^+$ binding and becoming a proton donor at physiological pH [51]. The n_{H+} values presented in Table 1 are compatible with Glu270 (-FVG**E**GI), a residue conserved in all sequences analysed (Fig. 1), functioning as proton acceptor during coenzyme binding, probably after the induced movement of the C-terminus [33].

Stability of a bent FAD conformation in bacterial FPRs was thought to depend on the interactions between its adenosine moiety and the C-terminal tail. However, removal of aminoacids beyond position 266 in *Rc*FPR shortened variants eliminates those interactions leaving the flavin in a more exposed situation without promoting significant changes in FAD conformation. In conclusion, our results signalise as the most significant roles for the C-terminal extension of bacterial FPRs: i) to expedite the entry and exit of the coenzyme modulating the strength of molecular linkages, ii) to support an efficient geometry of the *Rc*FPR:NADP$^+$ complex regulating flavin midpoint potential for optimal HT, and, finally, iii) to supply a C-terminal glutamate functioning as proton acceptor during catalysis of subclass I bacterial FPRs.

Acknowledgements

The authors acknowledge the funding from the Spanish MINECO (grants BIO2010-14983, BFU2011-25326 and CTQ2010-17476), the Aragonian Government DGA-FSE (grant B18), and the Argentinian CONICET (grant PIP 0365, 2012/14). A. S-A holds an FPU fellowship from the Spanish Ministry of Education and A. B. received a postdoctoral fellowship from Argentinean CONICET.

Appendix A. Supplementary data

Supplementary data to this article can be found online at http://dx.doi.org/10.1016/j.bbabio.2013.08.008.

References

[1] A.K. Arakaki, E.A. Ceccarelli, N. Carrillo, Plant-type ferredoxin-NADP$^+$ reductases: a basal structural framework and a multiplicity of functions, FASEB J. 11 (1997) 133–140.
[2] E.A. Ceccarelli, A.K. Arakaki, N. Cortez, N. Carrillo, Functional plasticity and catalytic efficiency in plant and bacterial ferredoxin-NADP(H) reductases, Biochim. Biophys. Acta 1698 (2004) 155–165.
[3] M. Medina, Structural and mechanistic aspects of flavoproteins: photosynthetic electron transfer from photosystem I to NADP$^+$, FEBS J. 276 (2009) 3942–3958.
[4] A.R. Krapp, R.E. Rodríguez, H.O. Poli, D.H. Paladini, J.F. Palatnik, N. Carrillo, The flavoenzyme ferredoxin (flavodoxin)-NADP(H) reductase modulates NADP(H) homeostasis during the soxRS response of *Escherichia coli*, J. Bacteriol. 184 (2002) 1474–1480.
[5] Y. Lee, S. Pena-Llopis, Y.S. Kang, H.D. Shin, B. Demple, E.L. Madsen, C.O. Jeon, W. Park, Expression analysis of the *fpr* (ferredoxin-NADP$^+$ reductase) gene in *Pseudomonas putida* KT2440, Biochem. Biophys. Res. Commun. 339 (2006) 1246–1254.
[6] M.L. Tondo, M.A. Musumeci, M.L. Delprato, E.A. Ceccarelli, E.G. Orellano, Structural-functional characterization and physiological significance of ferredoxin-NADP$^+$ reductase from *Xanthomonas axonopodis pv. citri*, PLoS One 6 (2011) e27124.
[7] N. Carrillo, E.A. Ceccarelli, Open questions in ferredoxin-NADP$^+$ reductase catalytic mechanism, Eur. J. Biochem. 270 (2003) 1900–1915.
[8] A. Aliverti, V. Pandini, A. Pennati, M. de Rosa, G. Zanetti, Structural and functional diversity of ferredoxin-NADP$^+$ reductases, Arch. Biochem. Biophys. 474 (2008) 283–291.
[9] N. Muraki, D. Seo, T. Shiba, T. Sakurai, G. Kurisu, Asymmetric dimeric structure of ferredoxin-NAD(P)$^+$ oxidoreductase from the green sulfur bacterium *Chlorobaculum tepidum*: implications for binding ferredoxin and NADP$^+$, J. Mol. Biol. 401 (2010) 403–414.
[10] M. Medina, M. Martínez-Júlvez, J.K. Hurley, G. Tollin, C. Gómez-Moreno, Involvement of glutamic acid 301 in the catalytic mechanism of ferredoxin-NADP$^+$ reductase from *Anabaena* PCC 7119, Biochemistry 37 (1998) 2715–2728.
[11] A. Aliverti, C.M. Bruns, V.E. Pandini, P.A. Karplus, M.A. Vanoni, B. Curti, G. Zanetti, Involvement of serine 96 in the catalytic mechanism of ferredoxin-NADP$^+$ reductase: structure-function relationship as studied by site-directed mutagenesis and X-ray crystallography, Biochemistry 34 (1995) 8371–8379.
[12] L. Piubelli, A. Aliverti, A.K. Arakaki, N. Carrillo, E.A. Ceccarelli, P.A. Karplus, G. Zanetti, Competition between C-terminal tyrosine and nicotinamide modulates pyridine nucleotide affinity and specificity in plant ferredoxin-NADP$^+$ reductase, J. Biol. Chem. 275 (2000) 10472–10476.
[13] J.T. Wan, J.T. Jarrett, Electron acceptor specificity of ferredoxin (flavodoxin):NADP$^+$ oxidoreductase from *Escherichia coli*, Arch. Biochem. Biophys. 406 (2002) 116–126.
[14] C. Bittel, L.C. Tabares, M. Armesto, N. Carrillo, N. Cortez, The oxidant-responsive diaphorase of *Rhodobacter capsulatus* is a ferredoxin (flavodoxin)-NADP(H) reductase, FEBS Lett. 553 (2003) 408–412.
[15] I. Nogués, I. Pérez-Dorado, S. Frago, C. Bittel, S.G. Mayhew, C. Gómez-Moreno, J.A. Hermoso, M. Medina, N. Cortez, N. Carrillo, The ferredoxin-NADP(H) reductase from *Rhodobacter capsulatus*: molecular structure and catalytic mechanism, Biochemistry 44 (2005) 11730–11740.
[16] M.A. Musumeci, H. Botti, A. Buschiazzo, E.A. Ceccarelli, Swapping FAD binding motifs between plastidic and bacterial ferredoxin-NADP(H) reductases, Biochemistry 50 (2011) 2111–2122.
[17] A. Wang, Y. Zeng, H. Han, S. Weeratunga, B.N. Morgan, P. Moenne-Loccoz, E. Schonbrunn, M. Rivera, Biochemical and structural characterization of *Pseudomonas aeruginosa* Bfd and FPR: ferredoxin NADP$^+$ reductase and not ferredoxin is the redox partner of heme oxygenase under iron-starvation conditions, Biochemistry 46 (2007) 12198–12211.
[18] C.J. Batie, H. Kamin, Electron transfer by ferredoxin:NADP$^+$ reductase. Rapid-reaction evidence for participation of a ternary complex, J. Biol. Chem. 259 (1984) 11976–11985.
[19] J.A. Hermoso, T. Mayoral, M. Faro, C. Gomez-Moreno, J. Sanz-Aparicio, M. Medina, Mechanism of coenzyme recognition and binding revealed by crystal structure analysis of ferredoxin-NADP$^+$ reductase complexed with NADP$^+$, J. Mol. Biol. 319 (2002) 1133–1142.
[20] J. Tejero, I. Pérez-Dorado, C. Maya, M. Martínez-Júlvez, J. Sanz-Aparicio, C. Gómez-Moreno, J.A. Hermoso, M. Medina, C-terminal tyrosine of ferredoxin-NADP$^+$ reductase in hydride transfer processes with NAD(P)$^+$/H, Biochemistry 44 (2005) 13477–13490.
[21] I. Lans, M. Medina, E. Rosta, G. Hummer, M. García-Viloca, J.M. Lluch, A. González-Lafont, Theoretical study of the mechanism of the hydride transfer between ferredoxin-NADP$^+$ reductase and NADP$^+$: the role of Tyr303, J. Am. Chem. Soc. 134 (2012) 20544–20553.
[22] M.A. Musumeci, A.K. Arakaki, D.V. Rial, D.L. Catalano-Dupuy, E.A. Ceccarelli, Modulation of the enzymatic efficiency of ferredoxin-NADP(H) reductase by the amino acid volume around the catalytic site, FEBS J. 275 (2008) 1350–1366.
[23] M. Medina, C. Gómez-Moreno, Interaction of ferredoxin-NADP$^+$ reductase with its substrates: optimal interaction for efficient electron transfer, Photosynth. Res. 79 (2004) 113–131.
[24] A. Sánchez-Azqueta, M.A. Musumeci, M. Martínez-Júlvez, E.A. Ceccarelli, M. Medina, Structural backgrounds for the formation of a catalytically competent complex with NADP(H) during hydride transfer in ferredoxin-NADP$^+$ reductases, Biochim. Biophys. Acta 1817 (2012) 1063–1071.
[25] I. Nogués, J. Tejero, J.K. Hurley, D. Paladini, S. Frago, G. Tollin, S.G. Mayhew, C. Gómez-Moreno, E.A. Ceccarelli, N. Carrillo, M. Medina, Role of the C-terminal tyrosine of ferredoxin-nicotinamide adenine dinucleotide phosphate reductase in the electron transfer processes with its protein partners ferredoxin and flavodoxin, Biochemistry 43 (2004) 6127–6137.
[26] J.R. Peregrina, A. Sánchez-Azqueta, B. Herguedas, M. Martínez-Júlvez, M. Medina, Role of specific residues in coenzyme binding, charge-transfer complex formation, and catalysis in *Anabaena* ferredoxin-NADP$^+$ reductase, Biochim. Biophys. Acta 1797 (2010) 1638–1646.
[27] V. Bianchi, P. Reichard, R. Eliasson, E. Pontis, M. Krook, H. Jornvall, E. Haggard-Ljungquist, *Escherichia coli* ferredoxin NADP$^+$ reductase: activation of *E. coli* anaerobic ribonucleotide reduction, cloning of the gene (*fpr*), and overexpression of the protein, J. Bacteriol. 175 (1993) 1590–1595.
[28] P.A. Karplus, C.M. Bruns, Structure-function relations for ferredoxin reductase, J. Bioenerg. Biomembr. 26 (1994) 89–99.
[29] L. Serre, F.M. Vellieux, M. Medina, C. Gómez-Moreno, J.C. Fontecilla-Camps, M. Frey, X-ray structure of the ferredoxin:NADP$^+$ reductase from the cyanobacterium *Anabaena* PCC 7119 at 1.8 Å resolution, and crystallographic studies of NADP$^+$ binding at 2.25 Å resolution, J. Mol. Biol. 263 (1996) 20–39.
[30] M. Ingelman, V. Bianchi, H. Eklund, The three-dimensional structure of flavodoxin reductase from *Escherichia coli* at 1.7 Å resolution, J. Mol. Biol. 268 (1997) 147–157.
[31] G. Sridhar Prasad, N. Kresge, A.B. Muhlberg, A. Shaw, Y.S. Jung, B.K. Burgess, C.D. Stout, The crystal structure of NADPH:ferredoxin reductase from *Azotobacter vinelandii*, Protein Sci. 7 (1998) 2541–2549.
[32] P.A. Karplus, H.R. Faber, Structural aspects of plant ferredoxin:NADP$^+$ oxidoreductases, Photosynth. Res. 81 (2004) 303–315.
[33] A. Bortolotti, I. Pérez-Dorado, G. Goñi, M. Medina, J.A. Hermoso, N. Carrillo, N. Cortez, Coenzyme binding and hydride transfer in *Rhodobacter capsulatus* ferredoxin/flavodoxin NADP(H) oxidoreductase, Biochim. Biophys. Acta 1794 (2009) 199–210.
[34] J.R. Peregrina, I. Lans, M. Medina, The transient catalytically competent coenzyme allocation into the active site of *Anabaena* ferredoxin-NADP$^+$ reductase, Eur. Biophys. J. 41 (2012) 117–128.
[35] D.H. Paladini, M.A. Musumeci, N. Carrillo, E.A. Ceccarelli, Induced fit and equilibrium dynamics for high catalytic efficiency in ferredoxin-NADP(H) reductases, Biochemistry 48 (2009) 5760–5768.
[36] J. Tejero, J.R. Peregrina, M. Martínez-Júlvez, A. Gutiérrez, C. Gómez-Moreno, N.S. Scrutton, M. Medina, Catalytic mechanism of hydride transfer between NADP$^+$/H and ferredoxin-NADP$^+$ reductase from *Anabaena* PCC 7119, Arch. Biochem. Biophys. 459 (2007) 79–90.
[37] A.W. Munro, M.A. Noble, Fluorescence analysis of flavoproteins, Methods Mol. Biol. 131 (1999) 25–48.
[38] F. Forneris, R. Orru, D. Bonivento, L.R. Chiarelli, A. Mattevi, ThermoFAD, a Thermofluor-adapted flavin ad hoc detection system for protein folding and ligand binding, FEBS J. 276 (2009) 2833–2840.
[39] R.N. Goldberg, N. Kishore, R.M. Lennen, Thermodynamic quantities for the ionization reactions of buffers, J. Phys. Chem. Ref. Data 31 (2002) 231–370.
[40] M. Martínez-Júlvez, M. Medina, A. Velázquez-Campoy, Binding thermodynamics of ferredoxin:NADP$^+$ reductase: two different protein substrates and one energetics, Biophys. J. 96 (2009) 4966–4975.
[41] T.G. Battye, L. Kontogiannis, O. Johnson, H.R. Powell, A.G. Leslie, iMOSFLM: a new graphical interface for diffraction-image processing with MOSFLM, Acta Crystallogr. D Biol. Crystallogr. 67 (2011) 271–281.
[42] P. Evans, Scaling and assessment of data quality, Acta Crystallogr. D Biol. Crystallogr. 62 (2006) 72–82.

[43] CCP4, The CCP4 suite: programs for protein crystallography, Acta Crystallogr. D Biol. Crystallogr. 50 (1994) 760–763.
[44] A. Vagin, A. Teplyakov, Molecular replacement with MOLREP, Acta Crystallogr. D Biol. Crystallogr. 66 (2010) 22–25.
[45] P.D. Adams, P.V. Afonine, G. Bunkoczi, V.B. Chen, I.W. Davis, N. Echols, J.J. Headd, L.W. Hung, G.J. Kapral, R.W. Grosse-Kunstleve, A.J. McCoy, N.W. Moriarty, R. Oeffner, R.J. Read, D.C. Richardson, J.S. Richardson, T.C. Terwilliger, P.H. Zwart, PHENIX: a comprehensive Python-based system for macromolecular structure solution, Acta Crystallogr. D Biol. Crystallogr. 66 (2010) 213–221.
[46] P. Emsley, K. Cowtan, Coot: model-building tools for molecular graphics, Acta Crystallogr. D Biol. Crystallogr. 60 (2004) 2126–2132.
[47] R.A. Laskowski, M.W. MacArthur, D.S. Moss, J.M. Thornton, PROCHECK: a program to check the stereochemical quality of protein structures, J. Appl. Crystallogr. 26 (1993) 283–291.
[48] V. Massey, The chemical and biological versatility of riboflavin, Biochem. Soc. Trans. 28 (2000) 283–296.
[49] I. Lans, J.R. Peregrina, M. Medina, M. García-Viloca, A. González-Lafont, J.M. Lluch, Mechanism of the hydride transfer between *Anabaena* Tyr303Ser FNR_{rd}/FNR_{ox} and $NADP^{+}$/H. A combined pre-steady-state kinetic/ensemble-averaged transition-state theory with multidimensional tunneling study, J. Phys. Chem. B 114 (2010) 3368–3379.
[50] V.I. Dumit, T. Essigke, N. Cortez, G.M. Ullmann, Mechanistic insights into ferredoxin-NADP(H) reductase catalysis involving the conserved glutamate in the active site, J. Mol. Biol. 397 (2010) 814–825.
[51] V.I. Dumit, A. Bortolotti, N. Cortez, G.M. Ullmann, NADP(H) Binding to Ferredoxin-NADP(H) Reductase from *Rhodobacter capsulatus*, and the Contribution of the Conserved Glutamate in the Active Site to the Process, in: S. Miller, R. Hille, B. Palfey (Eds.), Flavins and Flavoproteins 2011, Lulu, Raleigh, 2013, pp. 559–568.